In situ Atomic Force Microscopy study of dissolution of the barite (001) surface in water at 30℃

Kuwahara, Yoshihiro
Department of Environmental Changes, Faculty of Social and Cultural Studies, Kyushu University

出版情報：Geochimica et Cosmochimica Acta. 75 (1), pp.41-51, 2011-01-01. Elsevier
バージョン：

In situ Atomic Force Microscopy study of dissolution of the barite (001) surface in water at 30°C

Yoshihiro Kuwahara

Department of Environmental Changes, Faculty of Social and Cultural Studies,
Kyushu University, Motooka, Fukuoka 819-0395, Japan.
E-mail: ykuwa@scs.kyushu-u.ac.jp

Corresponding author:
Yoshihiro Kuwahara
Department of Environmental Changes, Faculty of Social and Cultural Studies, Kyushu University, Motooka, Fukuoka 819-0395, Japan.
E-mail: ykuwa@scs.kyushu-u.ac.jp
TEL:+81-92-802-5654
FAX:+81-92-802-5662

Abstract

The dissolution behavior of the barite (001) surface in pure water at 30°C was investigated using in situ Atomic Force Microscopy (AFM), to better understand the dissolution mechanism and the microtopographical changes that occur during the dissolution, such as steps and etch pits. The dissolution of the barite (001) surface started with the slow retreat of steps, after which, about 60 min later, the <*hk*0> steps of one unit cell layer or multi-layers became two-step fronts (fast "f" and slow "s" steps) with a half-unit cell layer showing different retreat rates. The "f" step had a fast retreat rate (≈ (14 ± 1) x 10^{-2} nm/sec) and tended to have a jagged step edge, whereas the "s" step (≈ (1.8 ± 0.1) x 10^{-2} nm/sec) had a relatively straight front. The formation of the "f" steps led to the formation of a new one-layer step, where the front of the "s" step was overtaken by that of the immediate underlying "f" step. The "f" steps also led to the decrease of the <*hk*0> steps and the increase in the percentage of stable steps parallel to the [010] direction during the dissolution.

Etch pits, which could be observed after about 90 min, were of three types: triangular etch pits with a depth of a half-unit cell, shallow etch pits, and deep etch pits. The triangular etch pits were bounded by the step edges parallel to [010], [120], and [1-20] and had opposite orientations in the upper half and lower half layers. Shallow etch pits that had a depth of two or more half-unit cell layers had any two consecutive pits pointing in the opposite direction of each other. The triangular etch pit appeared to grow by simultaneously removal of a row of ions parallel to each direction from the three step edges. At first, deep etch pits were elongated in the [010] direction with a curved outline and then gradually developed to an angular form bounded by the {100}, {310}, and (001) faces. The retreat rate of the (001) face was much slower than those of the {100} and {310} and tended to separate into two rates ((0.13 ± 0.01) x 10^{-2} nm/sec for the deep etch pits derived from a screw dislocation and (0.07 ± 0.01) x 10^{-2} nm/sec for those from other line defects).

The changes in the dissolution rate of a barite (001) surface during the dissolution

were estimated using the retreat rates and densities of the various steps as well as the growth rates, density, and areas of the lateral faces of the deep etch pits that were obtained from this AFM analysis. Our results showed that the dissolution rate of the barite (001) surface gradually increased and approached the bulk dissolution rate because of the change in the main factor determining the dissolution rate from the density of the steps to the growth and the density of the deep etch pits on the surface.

1. INTRODUCTION

Barite ($BaSO_4$) occurs in a wide variety of geologic environments that span geologic time from the Early Archean to the present (Hanor, 2000). On the one hand, most barite has been precipitated from aqueous fluids that contain barium derived from the alteration of silicate, carbonate, and sulfate minerals in various rocks. On the other hand, barite can dissolve during diagenesis and is unstable in reducing conditions; however, it is stable in oxidizing environments because of its low solubility (Hanor, 2000). Some of the dissolved Ba^{2+} may be used for reprecipitation of secondary barite or may be distributed in basinal water or meteoric groundwater (Hanor, 1994; Hanor, 2000). The dissolution and precipitation of barite, therefore, control the geochemical cycle of barium in surface water and in crustal fluids (Bosbach et al., 1998).

Barite is also a common scale-forming mineral because of its low solubility (K_{sp} = $10^{-9.99}$ at 25°C) in water, and its formation is almost inevitable and very troublesome in industrial water, oil, and gas production systems (Bosbach et al., 1998; Wang et al., 1999a and b; Risthaus et al., 2001; Becker et al., 2005). Some radioactive radium ions that are included in the well scale are removed from aqueous solutions during precipitation of the barite scale in oil field production because of the similarity in ionic radius and electronegativity to Ba^{2+} (Hanor, 2000). Water produced from their operations and released into the environment is likely to have substantial concentrations of dissolved Ba and Ra (Hanor, 2000).

Given the importance of barite dissolution in elucidating the processes and problems mentioned above, many experimental studies on barite dissolution have been performed, and the solubilities and dissolution rates, which were usually derived from macroscopic wet chemical data, have been reported (e.g., Blount, 1977; Raju and Atkinson, 1988; Christy and Putnis, 1993; Dove and Czank, 1995). These data, however, do not directly provide the dissolution mechanism. In situ Atomic Force Microscopy (AFM) studies on mineral dissolution make it possible to characterize the reactive surfaces on a site level and to estimate the retreat rates of steps and the growth rates of etch pits

(Bosbach et al., 2000; Becker et al., 2005; Kuwahara, 2008). Many AFM studies on the dissolution reaction of the barite (001) surface have been reported (e.g., Putnis et al., 1995; Dove and Platt, 1996; Bosbach et al., 1998; Higgins et al., 1998; Wang et al., 1999a and b; Higgins et al., 2000; Risthaus et al., 2001, Kowacz and Putnis, 2008). However, although data on the microscopic dissolution mechanisms of barite in aqueous salt or chelate solutions have been reported, information on such mechanisms in pure water is unexpectedly sparse. Details on the formation and growth rate of different types of etch pits and the retreat rate of the various steps during barite dissolution in water are not well understood.

In this study, the dissolution behavior of the barite (001) surface in pure water at 30°C was examined using in situ AFM observations. The main goals of this study were to comprehend the dissolution behavior of the barite (001) surface on a step or site level and to estimate rates of microscopic dissolution reactions (such as the formation and growth of etch pits and step retreats) that occur at the barite surface-water interface and change the overall dissolution rate of the barite (001) surface during the dissolution.

2. EXPERIMENTAL METHODS

The barite ($(Ba_{0.98}Ca_{0.01}Sr_{0.01})SO_4$) used for this study was obtained from the Stonehem Barite Deposit, Colorado, USA. The barite samples were optically clear, single crystals and were cleaved parallel to the (001) cleavage plane with a sharp knife blade immediately before the AFM observations. The crystallographic direction of the sample crystals was determined from the observed etch pits morphology (Bosbach et al., 1998; Risthaus et al., 2001).

Barite dissolution was observed with a Nanoscope III with a Multimode SPM unit (Digital Instruments) using a fluid cell with an air/fluid heater system (Kuwahara, 2008), operating in contact mode AFM (CMAFM) on a vibration isolation platform in a temperature- and humidity-controlled room. The barite samples were reacted with deionized water at 30°C (± 0.3°C). The temperature was controlled by an air/fluid heater (Bio-Heater (Veeco)) and a Thermal Applications Controller (Veeco) and was also monitored by a thermocouple thermometer (Cole-Parmer Instrument, Kuwahara, 2008). The deionized water flowed through the fluid cell at a constant rate of 0.01 ml/min controlled by a syringe pump. We also attempted the dissolution experiments at flow rate over 0.01 ml/min but could not obtain clear AFM images. The AFM images were taken at scan rates of 1 to 4 Hz (mainly 2 Hz) and scan lines of 512 x 512 using a J-head piezoelectric scanner (125 μm *XY* scans and 5 μm *Z* scan) and oxide-sharpened Si_3N_4 tip units. The set point was decreased as low as possible, and direct scanning on the observed surface was done for as short a time as possible to reduce the scan force and to minimize the effect of the tip on the sample surface. Incidentally, there was no difference in the growth rates of etch pits estimated from AFM images that were obtained either by direct scanning about every 15 minutes or 90 minutes. The longest experiment duration was over 600 minutes. The AFM image analysis on the retreat rate of steps and the growth rate of etch pits followed the methods of Kuwahara (2006). The error of the analysis was estimated to be less than 5%.

3. RESULTS

The dissolution of the barite (001) surface in pure water at 30°C could be divided into three stages. The first stage of the dissolution was characterized only by the retreat of various steps that were formed mechanically by the initial cleaving with the knife blade (Figure 1a). The initial steps were generally parallel to <*hk*0> (mainly <120>, <130>, <140>, and so on) and [010], but they did not appear to be necessarily oriented parallel to energetically favorable crystallographic directions, and slightly curved steps were also observed. The steps had heights corresponding to a half-*c* unit cell layer (3.6 Å), a single unit cell layer (7.2 Å), and multiple layers (mean 5 layers). However, the initial [010] step with a half-layer was hardly observed. As described in Table 1, the <*hk*0> steps with a half-layer were divided into two types: those with a fast retreat rate (≈ (14 ± 1) x 10^{-2} nm/sec; called "f" step hereafter) and those with a slow retreat rate (≈ (1.8 ± 0.1) x 10^{-2} nm/sec; called "s" step). Here, the "fast (f)" and "slow (s)" do not indicate that the step rates were reversed, such that the retreat rate is first fast and then slows and vice versa at a later time. The "f" and "s" steps each had constant retreat rates during the dissolution experiments. The retreat rates ((0.6 ~ 0.9 ± 0.1) x 10^{-2} nm/sec) of the steps with one layer and multiple layers were slower than those of the "s" steps with a half-layer (Table 1). No etch pits were formed on the barite (001) surface during the first stage.

During the second stage, the change in the retreat behavior from a <*hk*0> step with one layer to a "f" step with an upper half-unit cell layer and a "s" step with a lower half-unit cell layer was observed; furthermore, the formation of etch pits and the individual retreat of steps were also observed (Figure 1b and c). Figure 1b clearly reveals the difference in the behavior of the retreat between the "f" (corresponding to the a' step in the figure) and the "s" (corresponding to the a'' step in the figure) steps. The retreat of the "f" step was observed after about 60 min in all the experiments (Figure 2). The "f" step had a fast retreat rate (~ (14 ± 1) x 10^{-2} nm/sec) and tended to have a jagged step edge, whereas the "s" step had a slow retreat rate (~ (1.8 ± 0.1) x 10^{-2}

nm/sec) and a relatively straight front (Figure 1b and c, Figure 2, Table 1). Once the jagged "f" step (corresponding to the b' step in Figure 1b) reached the "s" step immediately above it (corresponding to the a'' step in Figure 1b), a new one-layer step (corresponding to the a''' step in Figure 1c) was formed. The retreat rate of the new one-layer step was estimated to be (2.3 ± 0.1) x 10^{-2} nm/sec, which was slightly faster than that of the "s" step (Figure 2 and Table 1).

The a' layer in Figure 1b had the "f" and "s" step fronts on the left side and right side of the layer, respectively. However, the underlying a" layer in Figure 1b had the "s" and "f" step fronts on the left side and right side of the layer, respectively, but the "f" step of the a" layer at first did not show the fast retreat because of the overlying a' layer. Once the "f" step front of the a" layer was exposed on the surface due to the removal of the overlying a' layer, it started the fast retreat (the a'' step in Figure 1d). Some of the steps seemed to be generally parallel to the [010] directions, repeating these behaviors (Figure 1d).

Etch pits were observed after about 90 min in all the experiments (Figure 1c). The etch pits seemed to be divided into three types: triangular etch pits with a depth of a half-unit cell, shallow etch pits, and deep etch pits (Figures 1d, 3a and b). The triangular etch pits were bounded by the step edges parallel to [010], [120], and [1-20] and showed opposite orientations in the upper half and lower half layers. Shallow etch pits had a depth of two or more half-unit cell layers, and any two consecutive pits pointed in the opposite direction of each other. The changing orientations of the triangular features can be explained by the presence of the two-fold screw axis normal to the (001) plane (Bosbach et al., 1998; Wang et al., 1999a; Risthaus et al., 2001). The initial, deep etch pits were elongated in the [010] direction with curved step edges.

The last stage of the dissolution (after 5~6 hours) was characterized by an increase of the stable steps parallel to the [010] direction, followed by a decrease of steps parallel to <*hk*0>, and the development of angular deep etch pits. Many of the steps with a half-layer or one layer parallel to <*hk*0> that were formed mechanically by the cleaving

with the knife blade seemed to disappear due to the fast dissolution rate or to become gradually parallel to the [010] direction during the dissolution (Figures 1, 3, and 4). Deep etch pits with curved step edges gradually developed an angular form that appeared to be bounded by the {100}, {310} and (001) faces (Figure 3d). The deep etch pits tended to be separated into two types according to their retreat rates of the (001) face (Figures 4 and 5).

4. DISCUSSION

4.1. Behavior of step retreats

During the first stage of the barite (001) surface dissolution, only the retreats of the various initial steps, which were formed mechanically by the cleaving with the knife blade, were observed. The <*hk*0> steps with a half-layer showed two retreat rates: (14 ± 1) x 10^{-2} nm/sec ("f" step) and (1.8 ± 0.1) x 10^{-2} nm/sec ("s" step) (Table 1). The retreat rate of the "s" step was nearly equal to that ((1.5 ± 0.1) x 10^{-2} nm/sec) of the [120] step of the half-layer, triangular etch pit, as described below. The retreat rates ((0.6 ± 0.1) x 10^{-2} nm/sec ~ (0.9 ± 0.1) x 10^{-2} nm/sec) of the <*hk*0> and [010] steps with one layer and multiple layers were slower than that of the "s" steps and were slightly slower than that ((0.95 ± 0.05) x 10^{-2} nm/sec) of the [010] step of the triangular etch pits.

During the second stage, the <*hk*0> steps with one layer changed to two half-layer steps, i.e., a "f" step with an upper half-unit cell layer and a "s" step with a lower half-unit cell layer (Figure 1b). The large difference in the retreat rates between the "f" and the "s" steps led to the formation of a new one-layer step, with the front of the "s" step overtaken by that of the immediately underlying "f" step (Figure 1c). However, none of the [010] steps with one layer showed this behavior.

In the AFM experiments, the retreat rate ((2.3 ± 0.1) x 10^{-2} nm/sec) of the new one-layer step tended to be slightly faster than that ((1.8 ± 0.1) x 10^{-2} nm/sec) of the "s" step with a half-layer (Figure 2 and Table 1). Similar results have been reported in the dissolution experiments of barite at elevated temperatures (Higgins et al., 1998). This slightly faster retreat rate of the new one-layer step may have been caused by the formation of a kink line, such as a wave-cut cliff, along the front of the step, due to the fast retreat of the front of the "f" lower half-layer.

The difference in retreat behaviors of the "f" and the "s" steps can be explained in Figure 6. Assuming that an upper half-layer of barite has two step fronts (step 1 and step 2 on the right side and left side, respectively, of the layer in Figure 6a) parallel to

the [120] direction on both sides of the layer, the retreat mechanisms of the two steps are expected to be different from each other. The dissolution of the steps would start by the removal of a Ba^{2+} at a high *z* position (*z* = 0) and the subsequent dissolution of a neighboring SO_4^{2-} at a high *z* position in the front of the steps to form the triangular etch pit mentioned below (Risthaus et al., 2001). As with step 1 in Figure 6a, the Ba^{2+} at a high *z* position that remains in the front would be dissolved following the removal of the pairs of Ba^{2+} and SO_4^{2-}, at the formation of the triangular etch pit. Similarly, the two Ba^{2+} and the neighboring SO_4^{2-} at a low *z* position (z = -0.18) in the front of the step would then be dissolved. Consequently, many jagged kink sites are produced in the front of step 1 and lead to the rapid removal of SO_4^{2-} that remains in the jagged front and the rapid formation of the next new front. In addition, some of step 1 may evolve more stable [010] steps (Figures 1d and 6a).

In contrast, with step 2 in Figure 6a, the ion at a high *z* position that remains in the front by the first removal of a pair of Ba^{2+} and SO_4^{2-} is SO_4^{2-} not Ba^{2+}, which is covered by the pair of Ba^{2+} and SO_4^{2-} located at a low *z* position in the front. The pair of the SO_4^{2-} that remains in the retreated front and the Ba^{2+} protected by the pair of Ba^{2+} and SO_4^{2-} located at a low *z* position is relatively stable. Therefore, the retreat of step 2 would be caused by the repetition of the relatively slow dissolution of pairs of one Ba^{2+} and one neighboring SO_4^{2-} at high or low *z* positions, producing a relatively straight front.

Although Figure 6 illustrates the difference in the retreat behavior on the [120] half-layer step, the behavior on the other <*hk*0> steps with a half-layer can also be explained in the same manner. In Figure 6a (on the upper half-layer), steps retreating roughly in the [160] or [1-60] direction, which corresponds to the advancing direction of the triangular etch pit corner, become the “f” step, whereas steps retreating in the opposite direction become the “s” step. For example, the two acute corners of the triangular etch pit formed on the a’ layer in Figure 1, point roughly to the right and top of the figure. Therefore, the step that retreats roughly to the right on the figure on the

left side of the a' layer in Figure 1 becomes the "f" step, but the step that retreats roughly to the left on the figure on the right side of the a' layer becomes the "s" step. Our AFM results show that the "f" step tends to have a jagged step edge but that the "s" step has a relatively straight front (Figures 1b, c), which strongly supports this model.

The new one-layer step does not show the splitting phenomenon unless the overlying "s" step is removed because the "s" step front blocks the fast retreat of the immediately underlying "f" step front. Once the front of the "f" lower half-layer (e.g., step 1 in Figure 6b) overlaid with the upper-half layer (e.g., step 2 in Figure 6a) is exposed on the surface due to the upper half-layer dissolution, the front of the "f" step suppressed by the upper half-layer starts the fast retreat (Figure 1d). These retreat patterns on the steps are consistent with the crystallographic orientation of the half-layer, triangular etch pit formed on the same layer, mentioned below (Figure 6).

When these retreat patterns on the steps are repeated, many of the initial steps with a half-layer or one layer parallel to <*hk*0> seem to disappear due to the fast dissolution rate or tend to change gradually to the [010] step during the dissolution (Figures 3 and 4). In addition, the growth of the triangular etch pits and shallow etch pits produce the new [010], [120], and [1-20] steps. Consequently, it is expected that the percentage of the stable steps parallel to the [010] direction increases at the last stage of the dissolution.

4.2. Formation and growth rate of triangular etch pits

No etch pits could be observed during the first stage (~60 min) of the barite dissolution in pure water at 30°C. The beginning of the formation of etch pits in these experiments was somewhat late relative to the previous reports (e.g., ~30 min in pure water at room temperature (Putnis et al., 1995; Bosbach et al., 1998)), which may be due to the differences in the (001) surface structure of different barite samples or to different experimental conditions. There is a possibility that the AFM tip influences the mineral surface during dissolution. To reduce the scan force and to minimize the

effect of the tip on the sample surface, the AFM observation, direct scanning on the observed surface was performed for as short a time as possible. We also confirmed that there were no differences in the growth rates of etch pits that were estimated from AFM images obtained by direct scanning about every 15 minutes or every 90 minutes. In addition, there was little difference in the step retreat rates in triangular etch pits in previous studies and in this study, despite the slow birth of etch pits in these experiments. The triangular etch pit was bounded by the steps parallel to [010], [120], and [1-20], and its growth was characterized by the retreat of the three steps (Figure 3c). The retreat rates of the [010] and [120] steps were estimated to be $(0.95 \pm 0.05) \times 10^{-2}$ nm/sec and $(1.5 \pm 0.1) \times 10^{-2}$ nm/sec, respectively (Figure 3c and Table 2). This shows that the spreading rate of the triangular pit was $(2.9 \pm 0.2) \times 10^{-2}$ nm/sec parallel to [010]. This result is very similar to an earlier result estimated under similar experimental conditions: Risthaus et al. (2001) reported that the lateral spreading rate of the triangular etch pit in pure water at room temperature was $(3 \pm 1) \times 10^{-2}$ nm/sec parallel to [010]. Therefore, this feature was probably intrinsic to our barite samples.

Figure 7 illustrates a model of the nucleation and the growth pattern of the triangular etch pits. According to Becker et al. (2005), the first ion to be dissolved in pure water would be most likely Ba^{2+} because the binding energies of Ba^{2+} and SO_4^{2-} to the lattice are comparable, but the hydration energy of Ba^{2+} in water is significantly higher than that for SO_4^{2-}. Removal of the Ba^{2+} is followed by the dissolution of a neighboring SO_4^{2-}, which is a fast step relative to the initial dissolution, and then dissolution of the next neighboring Ba^{2+}. However, most of the triangular etch pit may be related to point defects such as an atom vacancy or a substitutional impurity atom (e.g., Ba to Sr in barite) because the barite (001) surfaces sometimes appear to be quite stable (Bosbach et al., 1998), and the triangular etch pits do not show the retreat of the (001) plane. If the initial triangular etch pit that would be formed by the removal of two cations and one anion located at a high z position ($z = 0$ in Figure 7) in the upper half-layer grows by simultaneous removal of a row of ions parallel to each step

direction (a row of Ba^{2+} or SO_4^{2-} parallel to the [010] step and a row of Ba^{2+} and SO_4^{2-} parallel to the [120] and [1-20] steps), then the ratio of the retreated distance of the [120] and [010] steps becomes 1.55:1. The ratio is nearly equal to that (1.6:1) of the retreat rate of the [120] and [010] steps estimated from the AFM images (Table 2).

The half-layer, triangular etch pits showed opposite orientations in the upper half and lower half layers (Figure 1d). The changing orientations of the triangular features were consistent with the changing orientations of the steps between the upper and the lower half-layers, as mentioned above (Figure 6).

4.3. Formation and growth of deep etch pits

The formation of deep etch pits appeared to start during the second stage of the dissolution, as with the half-layer, triangular etch pits. The initial deep etch pits, however, tended to be elongated in the [010] direction with a curved outline, whereas the initial half-layer etch pits already appeared triangular as defined by the [010], [120], and [1-20] step edges (Figures 1 and 3). Such deep etch pits elongated in the [010] direction with curved outlines have also been reported in previous studies, but the experimental conditions were different from this study (e.g., in 0.1 M NaCl solution in Risthaus et al. (2001); in pure water at 60°C; and in 0.05 M NaCl or KCl solution in Kowacz and Putnis (2008)). The morphological change to angular deep etch pits appeared to occur gradually during the second and last stages of dissolution.

The angular, deep etch pits appeared to be bounded by the {100}, {310}, and (001) faces (Figure 3d), although the AFM cannot distinguish closely spaced steps from a true facet in the pit. Here, we characterized the growth of the deep etch pits by the retreat of their faces so that they could be compared with the results in previous AFM studies. The deep etch pits that form in pure water seemed to vary in morphology with temperature. For example, Bosbach et al. (1998) reported that the morphology of deep etch pits at room temperature (25°C) was defined by the {100} and {210} faces, which are the two lowest energy surfaces in barite crystals (Allan et al., 1993; Redfern and

Parker, 1998), and Kowacz and Putnis (2008) showed that the shape of the deep etch pits changed from hexagonal at 35°C to bow-shaped at 60°C. The angular deep etch pits in this study, which were bounded by the {100} and {310} faces, may be an intermediate form between the deep etch pits that are bounded by the {100} and {210} faces at low temperature and the bow-shaped, deep etch pits formed at higher temperature.

The origin of the deep etch pits, in all likelihood, was a line defect such as a screw dislocation or an edge dislocation. Our AFM observations revealed that a deep etch pit originated from a screw dislocation point ("S" in Figure 4a). The deep etch pits occurred not only sporadically but also along a line (Figure 4). The formation of such deep etch pits along a line may be related to the lineage structure (Klein, 2002).

The deep etch pits tended to have two retreat rates for the (001) plane, whereas they had one retreat rate each for the (100) face, (310) face, and [010] corner ($(0.7 \pm 0.1) \times 10^{-2}$ nm/sec, $(2.0 \pm 0.3) \times 10^{-2}$ nm/sec, and $(3.5 \pm 0.1) \times 10^{-2}$ nm/sec, respectively) (Figure 5 and Table 3). The (001) retreat rate ($(0.13 \pm 0.01) \times 10^{-2}$ nm/sec) of the deep etch pit, which is derived from a screw dislocation, tended to be about twice that ($(0.07 \pm 0.01) \times 10^{-2}$ nm/sec) of the deep etch pits derived from other line defects (probably edge dislocation). Many of the steps originating from the screw dislocation points on the barite (001) surface had a height of a unit cell (about 7.2 Å). Therefore, the retreat of the deep etch pits' (001) face that was derived from a screw dislocation would occur every one-unit cell layer. However, the retreat of the other deep etch pits must occur every one half-unit cell layer in the same way as the triangular etch pits or shallow etch pits; this retreat rate would need to be half as fast as the retreat of the deep etch pits derived from a screw dislocation. The two retreat rates of the deep etch pits' (001) plane were extremely slow relative to the lateral spreading rates of the other faces ($r_{[010]} : r_{(310)} : r_{(100)} : r_{(001)}$ = 26.3:15:5.5:1 or 52.5:30:11:1, where $r_{(hkl)}$ and $r_{[010]}$ indicate the retreat rates of the (*hkl*) face and [010] corner of the deep etch pit, respectively). Incidentally, the dissolution of one layer or one half-layer from a screw dislocation or

other line defect, respectively, was estimated to start about every 9 min. To the best of our knowledge, there is no other reports on the growth rate of the deep etch pits under similar conditions.

4.4. Change in the dissolution rate of the barite (001) surface

Understanding the dissolution rate on each barite crystal surface is indispensable for understanding macroscopic dissolution rates, although we cannot estimate the bulk dissolution rate of barite by the AFM data alone. In addition, it is very important to find the change in the barite cleavage surface dissolution rates during the dissolution because fresh cleavage surfaces of barite are easily formed in nature, although the barite (001) surfaces used in this study were cleaved with a knife blade, and the barite dissolution in this study probably did not reach steady state. Here, we attempted to roughly estimate the change in the barite (001) surface dissolution rate during the three stages of the dissolution. Table 4 shows the dissolution rates after 11 min as well as 5 and 10 hr estimated from the data on various steps and deep etch pits on a barite (001) surface area of 20 μm x 20 μm in Figure 4. Although the total dissolution rates of the barite (001) surface increased from 7.8 x 10^{-10} mol m^{-2} sec^{-1} to 4.1 x 10^{-9} mol m^{-2} sec^{-1} after 10 hr, these rates are considerably slower than the bulk dissolution rate reported in a previous study (7.9 x 10^{-8} mol m^{-2} sec^{-1} in pure water at 30°C (Dove and Czank, 1995)). This slowness was probably due to the stronger resistance of the barite (001) surface to the dissolution reaction in water than the other faces, as shown by the retreat rate of the deep etch pits' (001) face being much slower than the lateral spreading rates of the deep etch pits.

The dissolution rates of the barite (001) surface after 11 min (the first stage) and 5 hours (the second stage) were similar, but the details of the dissolution rates were different from each other (Table 4). The dissolution rate of the barite (001) surface after 11 min was basically only related to the retreat of the various steps due to the non-formation of etch pits; however, after 5 hr, the effect of the deep etch pits on the

dissolution increased, and the effect of the steps on the dissolution decreased because the step density decreased. Many of the <*hk*0> steps formed mechanically by the cleaving with the knife blade gradually decreased, and the deep etch pits formed on the barite (001) surface increased during the dissolution. This tendency became stronger in the dissolution after 10 hr (the last stage) (Table 4). These results indicate that the dissolution rate of the barite (001) surface in pure water at 30°C was controlled by the density of steps on the surface during the first stage, whereas it was mainly controlled by the growth and density of the deep etch pits during the late stage. The growth and increasing density of the deep etch pits during the last stage of the dissolution caused the increase in the lateral faces' area such as the {100} and {310}, which have fast retreat rates and therefore led to the increase of the dissolution rate. The more line defects (such as screw and edge dislocations), which are the origin of the deep etch pits, the barite (001) surface has, the more rapid the dissolution rate becomes, and the closer the dissolution rate is to the bulk dissolution rate.

5. CONCLUSIONS

This in situ AFM study of the barite (001) surface dissolution in pure water at 30°C revealed how the steps on the surface behaved during the dissolution, how the formation and growth of the half-layer and deep etch pits occurred and developed, and how the steps and etch pits influenced the dissolution rate of the barite (001) surface. The retreat rates of the various steps and the growth rates of the triangular etch pits and deep etch pits formed on the surface were estimated by the AFM analysis. Our in situ AFM observations revealed that the <*hk*0> step with one layer changed to two half-layer steps: a "f" step with a jagged front and a "s" step with a relatively straight front. In addition, a model that explains the difference in the behavior of the retreat between the "f" and the "s" steps was proposed. The AFM study also showed the growth pattern of the triangular etch pits and the morphological development of the deep etch pits to an angular form and revealed that the deep etch pit originating from a screw dislocation had a (001) face retreat rate that was twice as fast as the deep etch pits originating from other line defects. We also observed that many of the initial steps gradually decreased and the deep etch pits increased during the dissolution. Using the data, such as the retreat rates and density of the steps and the growth rates and density of the deep etch pits that were estimated from this AFM analysis, we estimated the change in the dissolution rate of the barite (001) surface during the dissolution. As a consequence, we demonstrated that the barite (001) surface dissolution rate was controlled by the density of steps on the surface during the first stage, whereas it was controlled by the growth and density of the deep etch pits during the late stage.

Acknowledgments. The author is grateful to Drs S. Uehara and K. Ishida of Kyushu University for their helpful suggestions. I also want to thank the three anonymous reviewers and the editor Kevin Rosso for their thorough reviews that improved the quality of the study. This study was supported in part by the Grant-in-Aid for Scientific Research (Y. Kuwahara, No. 17540457) from the Japan Society for the Promotion of Science.

References

Allan N.L., Rohl A.L., Gay D.H., Catlow C.R.A., Davey R.J. and Mackrodt W.C. (1993) Calculated bulk and surface-properties of sulfates. *Faraday Discuss*. **95**, 273-280.

Becker U., Biswas S., Kendall T., Risthaus P., Putnis C.V. and Pina C.M. (2005) Interactions between mineral surfaces and dissolved species: from monovalent ions to complex organic molecules. *Am. J. Sci*. **305**, 791-825.

Blount C.W. (1977) Barite and thermodynamic quantities up to 300°C and 1400 bars. *Am. Mineral*. **62**, 942-957.

Bosbach D, Hall C. and Putnis A. (1998) Mineral precipitation and dissolution in aqueous solution: in-situ microscopic observations on barite (001) with atomic force microscopy. *Chem. Geol.* **151**, 143-160.

Bosbach D., Charlet L., Bickmore B., and Hochella Jr. M.F. (2000) The dissolution of hectorite: In-situ, real-time observations using atomic force microscopy. *Am. Mineral*. **85**, 1209–1216.

Christy A.G. and Putnis A. (1993) The kinetics of barite dissolution and precipitation in water and sodium chloride brines at 44-85°C. *Geochim. Cosmochim. Acta* **57**, 2161-2168.

Dove P.M. and Czank C.A. (1995) Crystal chemical controls on the dissolution kinetics of the isostructural sulfates: Celestite, anglesite, and barite. *Geochim. Cosmochim. Acta* **59**, 1907-1915.

Dove P.M. and Platt F.M. (1996) Compatible real-time rates of mineral dissolution by Atomic Force Microscopy (AFM). *Chem. Geol*. **127**, 331-338.

Hanor J.S. (1994) Origin and migration of subsurface sedimentary basins. In *Geofluids: Origin and Migration of Fluids in Sedimentary Basins* (ed. J. Parnell). The Geological Society of London, Special Publication **78**, 151-174.

Hanor J.S. (2000) Barite-Celestine geochemistry and environments of formation. In *Reviews in Mineralogy and Geochemstry: Sulfate minerals – Crystallography,*

geochemistry, and environmental significance, vol. 40 (eds. C.N. Alpers, J.L. Jambor and D.K. Nordstrom). The Mineralogical Society of America, Washington, DC, pp. 193-275.

Higgins S.R., Jordan G and Eggleston C.M. (1998) Dissolution kinetics of the barium sulfate (001) surface by hydrothermal atomic force microscopy. *Langmuir* **14**, 4967-4971.

Higgins S.R., Bosbach D., Eggleston C.M. and Knauss K.G. (2000) Kink dynamics and step growth on barium sulfate (001): A hydrothermal scanning probe microscopy study. *J. Phys. Chem. B* **104**, 6978-6982.

Hill R.J. (1977) A furtherrefinement of the barite structure. *Canadian Mineral*. **15**, 522-526.

Klein C. (2002) *The 22nd Edition of the Manual of Mineral Science*. John Wiley & Sons, New York.

Kowacz M. and Putnis A. (2008) The effect of specific background electrolytes on water structure and solute hydration: Consequences for crystal dissolution and growth. *Geochim. Cosmochim. Acta* **72**, 4476-4487.

Kuwahara Y. (2006) In-situ AFM study of smectite dissolution under alkaline conditions at room temperature. *Am. Mineral*. **91**, 1142–1149.

Kuwahara Y. (2008) In situ observations of muscovite dissolution under alkaline conditions at 25–50 °C by AFM with an air/fluid heater system. *Am. Mineral*. **93**, 1209–1216.

Putnis A., Junta-Rosso J.L. and Hochella Jr. M.F (1995) Dissolution of barite by a clelating ligand: An atomic force microscopy study. *Geochim. Cosmochim. Acta* **59**, 4623-4632.

Raju K. and Atkinson G. (1988) Thermodynamics of "scale" mineral solubilities. 1. $BaSO_4$(s) in H_2O and aqueous NaCl. *J. Chem. Eng. Data* **33**, 490-495.

Redfern S.E. and Parker S.C. (1998) Atomistic simulation of the effects of calcium and strontium defects on the surface structure and stability of $BaSO_4$. *J. Chem. Soc.*

Faraday Trans. **94**, 1947-1952.

Risthaus P., Bosbach D., Becker U. and Putnis A. (2001) Barite scale formation and dissolution at high ionic strength studied with atomic force microscopy. *Coll. Surf.* **191**, 201-214.

Wang K.S., Resch R., Koel B.E., Shuler P.J., Tang Y. and Chen H.J. (1999a) Study of the dissolution of the barium sulfate (001) surface with hydrochloric acid by atomic force microscopy. *J. Coll. Interf. Sci*. **219**, 212-215.

Wang K.S., Resch R., Dunn K., Shuler P., Tang Y., Koel B.E. and Yen T.F. (1999b) Dissolution of the barite (001) surface by the chelating agent DTPA as studied with non-contact atomic force microscopy. *Coll. Surf*. **160**, 217-227.

Table 1 Average retreat rates of various steps on the barite (001) surface.

Step on the (001) surface	<hk0>[a] "f" step with half-layer[b]	<hk0> "s" step with half-layer[b]	<hk0> step with one layer (in the first stage)[b]	<hk0> step with one layer ("s" upper half-layer + "f" lower half-layer)[b]	[010] step with one layer	[010] step with multiple layers
Retreat rate (10^{-2} nm/sec)	14 ± 1	1.8 ± 0.1	0.9 ± 0.1	2.3 ± 0.1	0.8 ± 0.1	0.6 ± 0.1

(a) <120>, <130>, <140> steps, and so on, formed on the (001) surface by cleaving with knife.

(b) See Figures 1 and 2

(c) Average: 5 layers

Table 2 Average growth rate of triangular etch pits (See Figure 3).

Step or edge in etch pits	[010] step	[120] or [1-20] step
Retreat rate (x 10^{-2} nm/sec)	0.95 ± 0.05	1.5 ± 0.1

Table 3 Average growth rate of deep etch pits (See Figure 3).

Face or corner in etch pits	(100)	(310)	[010] corner	(001)
Retreat rate (x 10^{-2} nm/sec)	0.7 ± 0.1	2.0 ± 0.3	3.5 ± 0.2	0.13 ± 0.01 or 0.07 ±0.01

Table 4. Change in the dissolution rate of a barite (001) surface with time

	11 min	5 hr	10 hr
Density of <hk0> "f" half-layer step (nm/μm^2)	219	102	36
Density of <hk0> "s" half-layer step[a] (nm/μm^2)	339	184	164
Density of <hk0> one layer step (nm/μm^2)	378	124	34
Density of <hk0> multiple layer step[b] (nm/μm^2)	79	40	32
Density of [010] half and one layer step[a] (nm/μm^2)	215	218	195
Density of [010] multiple layer step[b] (nm/μm^2)	536	530	529
Dissolution rate for the steps[c] (mol m^{-2} sec^{-1})	7.8 x 10^{-10}	4.8 x 10^{-10}	3.8 x 10^{-10}
Density of deep etch pits (pits/μm^2)		0.1	0.2
Mean total area of {310} faces in a deep etch pit[c] (nm^3)		5004	28559
Mean total area of {100} faces in a deep etch pit[c] (nm^3)		5740	56619
Mean depth of deep etch pits (nm)		5.8	17.3
Dissolution rate for deep etch pits[c] (mol m^{-2} sec^{-1})		2.7 x 10^{-10}	3.7 x 10^{-9}
Total dissolution rate[c] (mol m^{-2} sec^{-1})	7.8 x 10^{-10}	7.5 x 10^{-10}	4.1 x 10^{-9}

(a) The [120] and [010] steps in the triangular etch pits were taken into the <*hk*0> "s" half-layer step and [010] half-layer step, respectively.

(b) Average: 5 layers

(c) Using a = 8.884 Å, b = 5.456 Å, c = 7.157 Å and density = 4.50 g/cm^3 (Hill, 1977). Here, the deep etch pit is considered to be bounded by the {100}, {310}, and (001) faces, and its growth is characterized by the retreat of the three faces.

Figure Caption

Figure 1. The sequence of the CMAFM height images of a barite (001) surface in pure water at 30°C after 9 min (a), 73 min (b), 99 min (c), and 212 min (d). See Figure 2 for the a, a', a'', and a''' steps and others in this figure. The black arrows show the direction and relative rate of the retreat of steps. During the first stage of the dissolution (a), only a slow retreat of steps (e.g., a and b step) occurs. In (b), a CMAFM deflection image (in the white box) that was obtained simultaneously is overlapped to clearly reveal the difference in the behavior of the retreat between the "fast (f)" step with an upper half of a unit cell layer and the "slow (s)" step with a lower half of a unit cell layer. The retreat of the "f" step could be observed after about 60 min (See Figure 2). Etch pits could be observed after about 90 min (c). In (d), triangular etch pits with a depth of a half of a unit cell that have opposite orientations in the upper half and lower half layers, due to the 2_1 screw axis, and deep etch pits elongated to the [010] direction can be seen.

Figure 2. Changes in the retreat rate of a [140] step (the "a" step in Figure 1) as a function of time. "A step with one layer ("f" step with an upper half-layer + "s" step with a lower half-layer)" in this figure corresponds to the "a" step in Figure 1(a). Also, the "f" step with an upper half-layer, "s" step with a lower half-layer, and new step with one layer ("s" step with an upper half-layer + "f" step with a lower half-layer) correspond to the a', a'', and a''' steps, respectively, in Figure 1.

Figure 3. (a) and (b) CMAFM height images of a barite (001) surface in pure water at 30°C after 360 min and 464 min, respectively. Three different etch pits can be observed: (1) triangular etch pits with a depth of a half of a unit cell that are bounded by three steps parallel to [010], [120], and [1-20]; (2) shallow etch pits with any two consecutive pits pointing in the opposite direction of each other; and

(3) deep etch pits elongated in the [010] direction. (c) The growth pattern of a triangular etch pit estimated from in situ AFM observations. The symbol "*r*" indicates the retreat rate of each step of the triangular pit. (d) The magnified CMAFM image of part (d) in Figure 3(b) showing morphological development of a deep etch pit from an earlier etch figure (corresponding to the deep etch pit in (a)) with curved step edges (outlined by a dotted line) to a later angular form bounded by the {100} and {310} faces. The white arrows show the direction and relative retreat rates of each step or corner of the pit.

Figure 4. CMAFM deflection images of a barite (001) surface in pure water at 30°C after 11 min (a), 311 min (b), and 600 min (c). The symbol "S" indicates a screw dislocation point and a deep etch pit derived from the point. The black arrows indicate a chain of deep etch pits that was probably derived from a row of line defects spaced at irregular intervals (lineage structure). Deep etch pits derived from a screw dislocation tended to be deeper than those derived from other line defects (probably edge dislocation) (see Figure 5).

Figure 5. A comparison of the retreat rates of the (001) face in deep etch pits derived from a screw dislocation (solid circle) and from another line defect (open circle). A deep etch pit derived from a screw dislocation has about twice the (001) retreat rate of that derived from other line defects.

Figure 6. A model illustrating the difference in the behavior of the retreat between "f" and "s" steps parallel to [120]. (a) and (b) The structures of an upper half-layer and a lower half-layer, respectively, of a unit cell of barite projected onto (001). The large and small black spheres indicate Ba^{2+} at a high z position ($z = 0$) and a low z position ($z = -0.18$), respectively. SO_4^{2-} at high and low z positions are also shown by the large and small tetrahedra, respectively. The initial triangular

etch pits that have opposite orientations in the upper (a) and lower (b) half-layers are also shown. When a pair of Ba^{2+} and SO_4^{2-} at a high *z* position in the initial front of the [120] step are removed, the ion that is located at a high *z* position in the retreated front of the step, is SO_4^{2-} (in the open circle on the left side of Figure 6(a)); however, in the step on the right side of the figure, is Ba^{2+} is present (in the open circle), which would be dissolved next. The step on the right side of Figure 6(a) would retreat fast due to the continuous and relatively easy formation of a kink, which tends to have a jagged front, whereas the step on the left side would retreat slowly by removing pairs of Ba^{2+} and SO_4^{2-} at a high *z* position and then pairs of these ions at a low *z* position; thus, the front tends to be straight. The steps show opposite orientations in the upper (a) and lower (b) half-layers because of the 2_1 screw axis normal to the (001) plane.

Figure 7. Schematic diagram of the growth pattern of a triangular etch pit depicted on the [001] projection of the structure of "an upper half-layer of a unit cell" of barite. The large and small black spheres indicate Ba^{2+} at a high *z* position ($z = 0$) and a low *z* position ($z = -0.18$), respectively. SO_4^{2-} at high and low *z* positions are also shown by the large and small tetrahedra, respectively. The arrows (a) and (b) indicate the retreated distance of the steps parallel to [120] and [010], respectively. Assuming that each step retreats by simultaneous removal of a row of ions parallel to the step direction (a row of Ba^{2+} and SO_4^{2-} parallel to the [120] and [1-20] steps and a row of Ba^{2+} or SO_4^{2-} parallel to the [010] step), the ratio of the retreated distance of (a) and (b) ((a) : (b) = 1.55:1) nearly equals the ratio of the retreat rate of those estimated from AFM analysis (see Table 1).

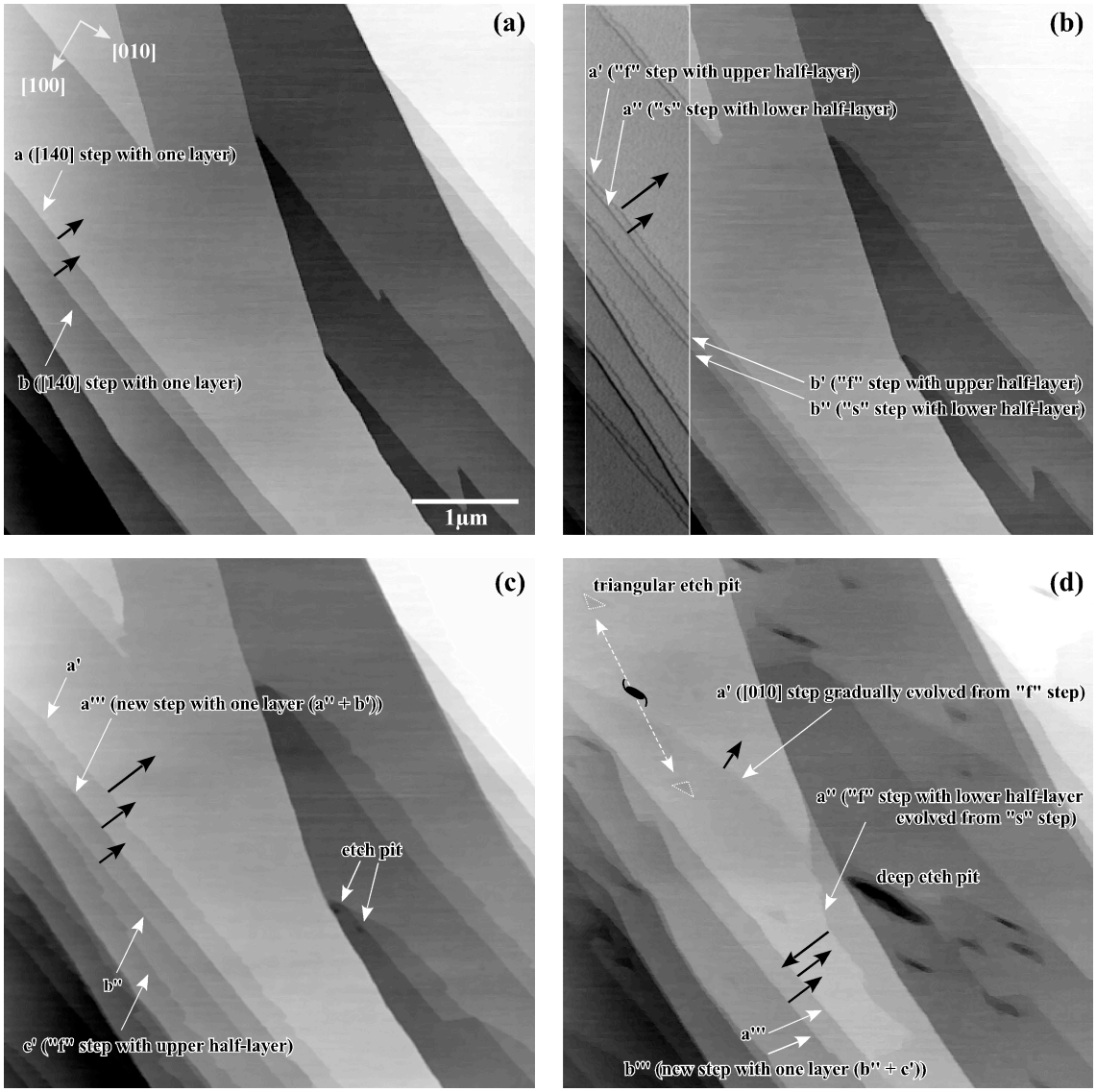
(a)
[010]
[100]
a ([140] step with one layer)
b ([140] step with one layer)
1µm
(b)
a' ("f" step with upper half-layer)
a'' ("s" step with lower half-layer)
b' ("f" step with upper half-layer)
b'' ("s" step with lower half-layer)
(c)
a'
a''' (new step with one layer (a'' + b'))
etch pit
b''
c' ("f" step with upper half-layer)
(d)
triangular etch pit
a' ([010] step gradually evolved from "f" step)
a'' ("f" step with lower half-layer evolved from "s" step)
deep etch pit
a'''
b''' (new step with one layer (b'' + c'))

Figure 1.

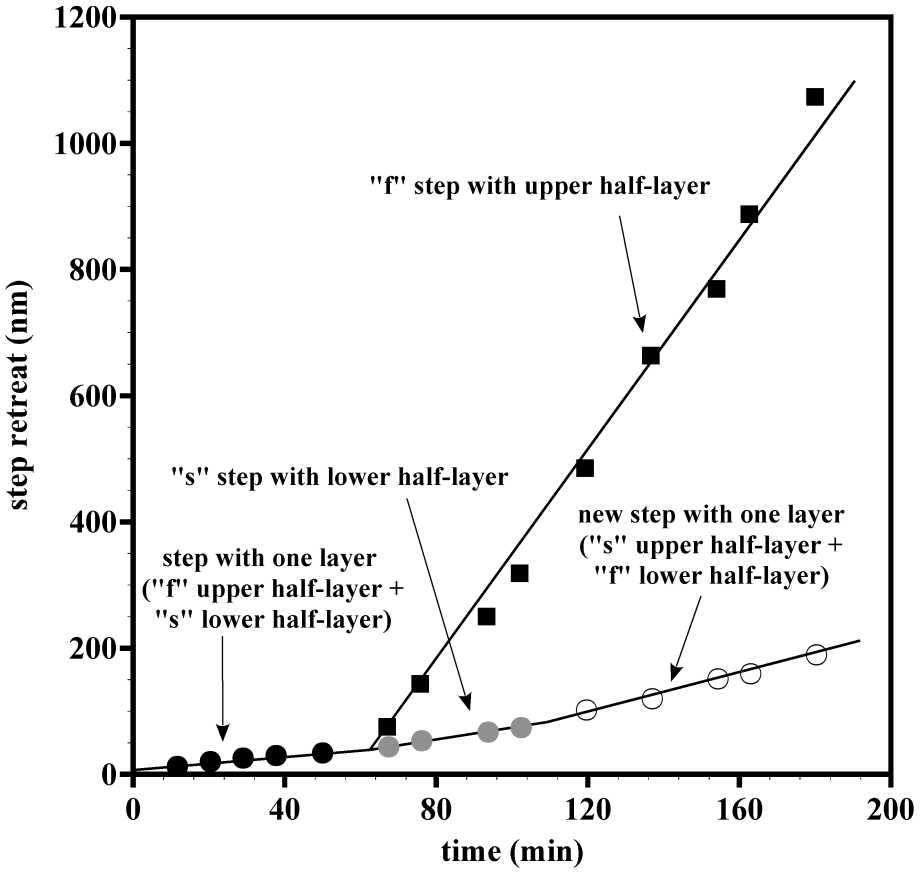
1200
1000
800
600
400
200
0
step retreat (nm)
0
40
80
120
160
200
time (min)
"f" step with upper half-layer
"s" step with lower half-layer
step with one layer
("f" upper half-layer +
"s" lower half-layer)
new step with one layer
("s" upper half-layer +
"f" lower half-layer)

Figure 2.

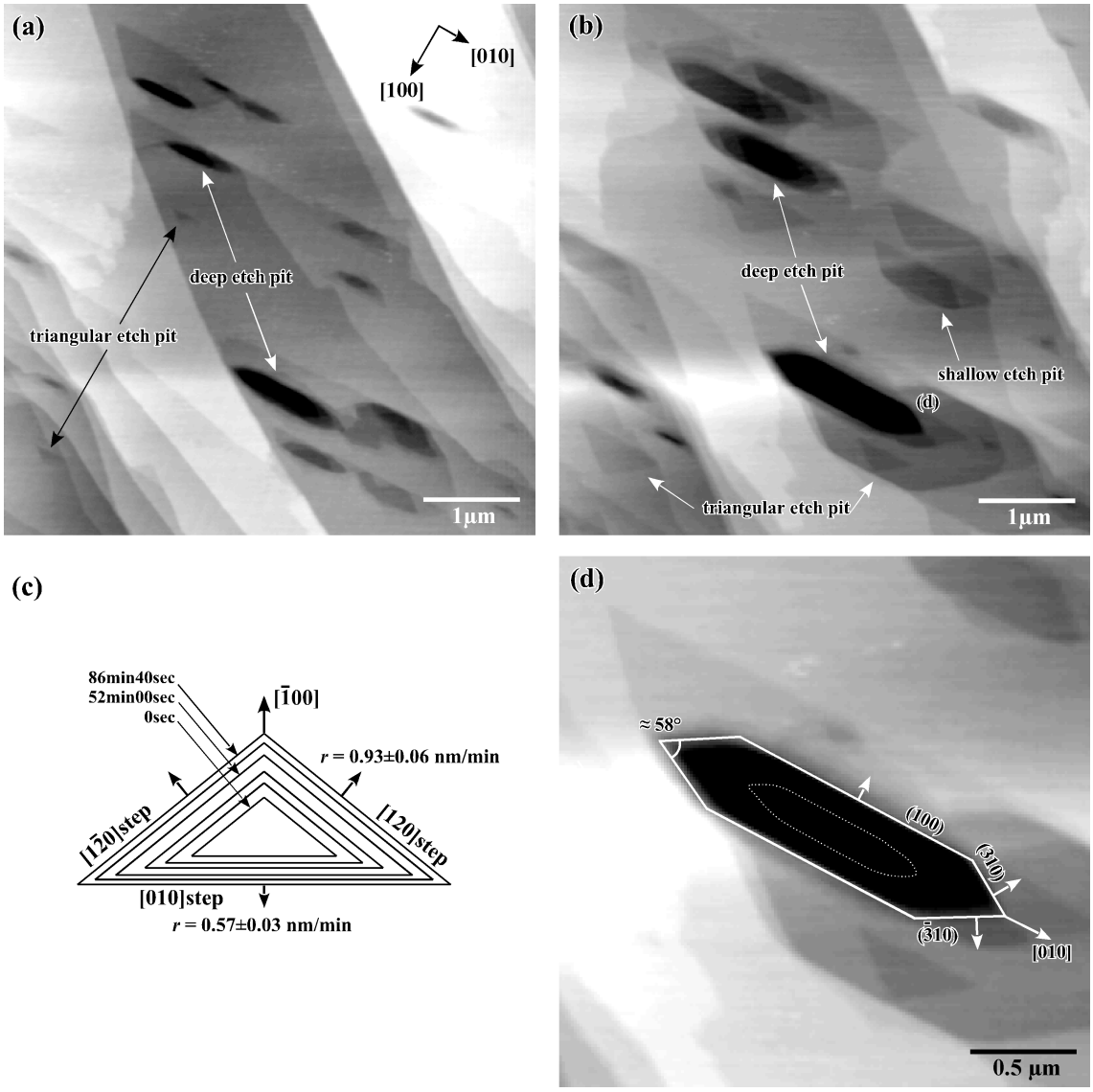
(a)
[010]
[100]
deep etch pit
triangular etch pit
1μm
(b)
deep etch pit
shallow etch pit
(d)
triangular etch pit
1μm
(c)
86min40sec
52min00sec
0sec
[1̄00]
r = 0.93±0.06 nm/min
[12̄0]step
[120]step
[010]step
r = 0.57±0.03 nm/min
(d)
≈ 58°
(100)
(310)
(3̄10)
[010]
0.5 μm

Figure 3.

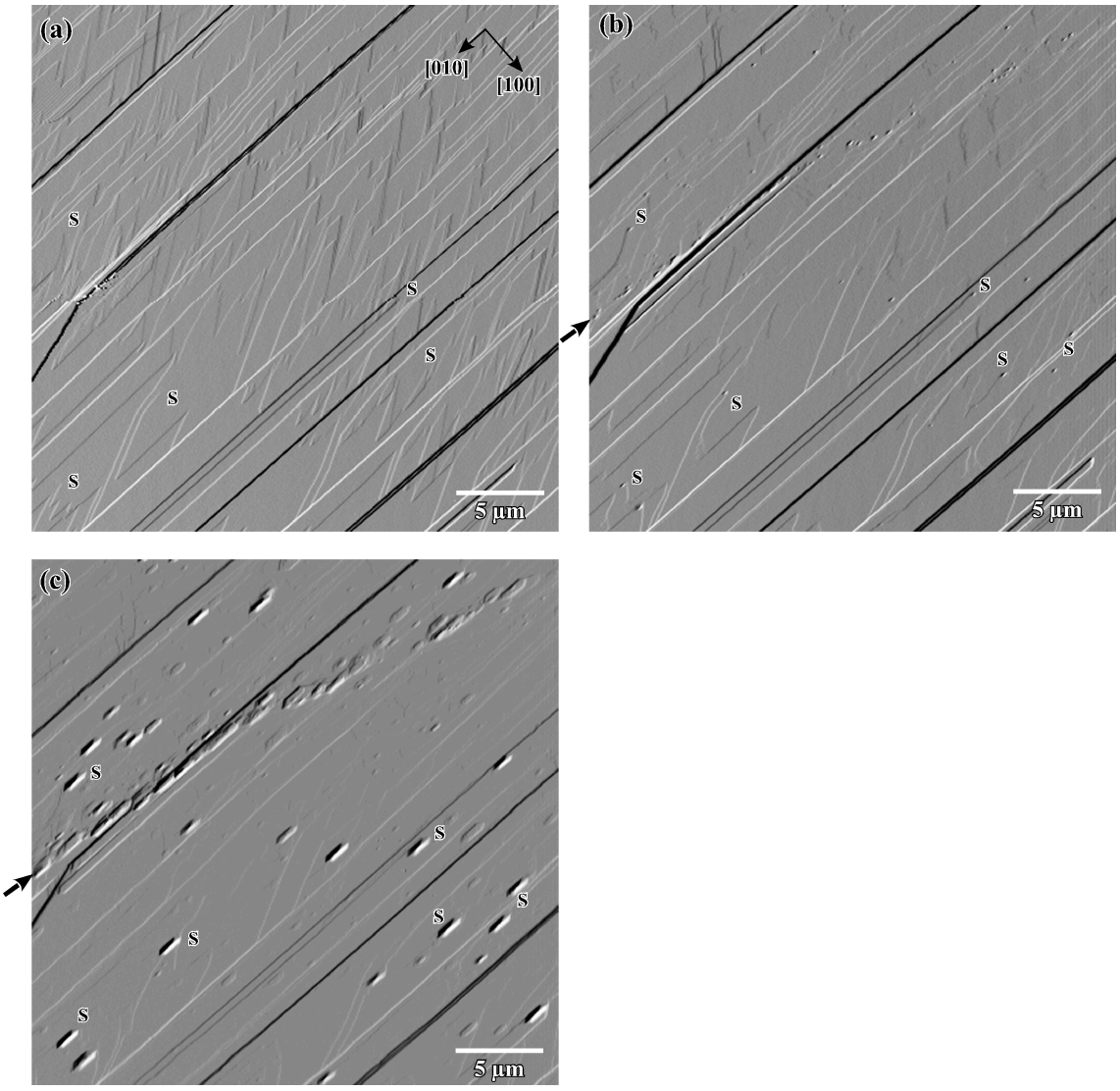

Figure 4.

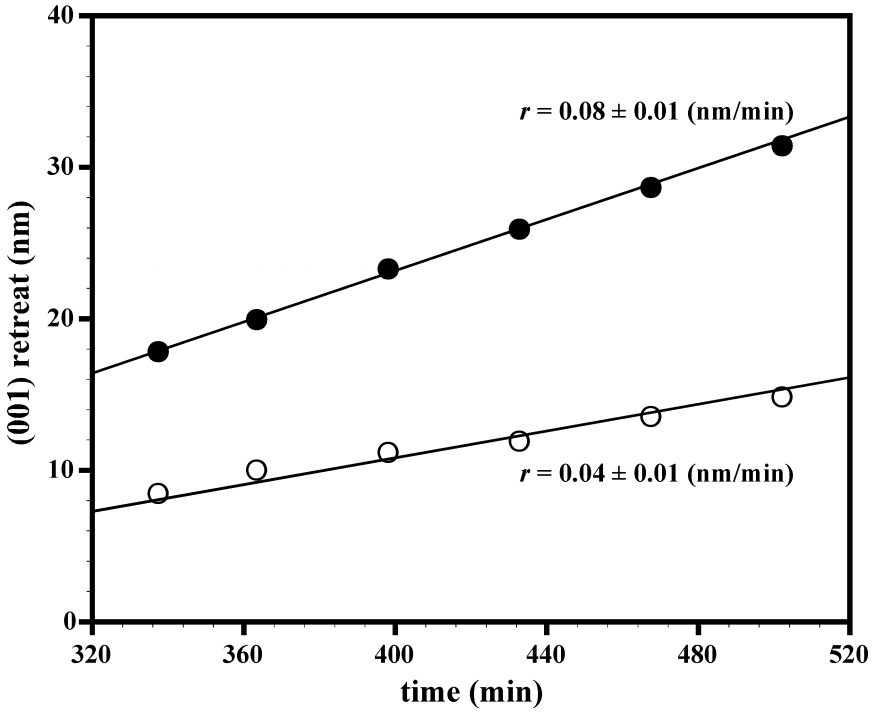
40
30
20
10
0
(001) retreat (nm)
320
360
400
440
480
520
time (min)
r = 0.08 ± 0.01 (nm/min)
r = 0.04 ± 0.01 (nm/min)

Figure 5.

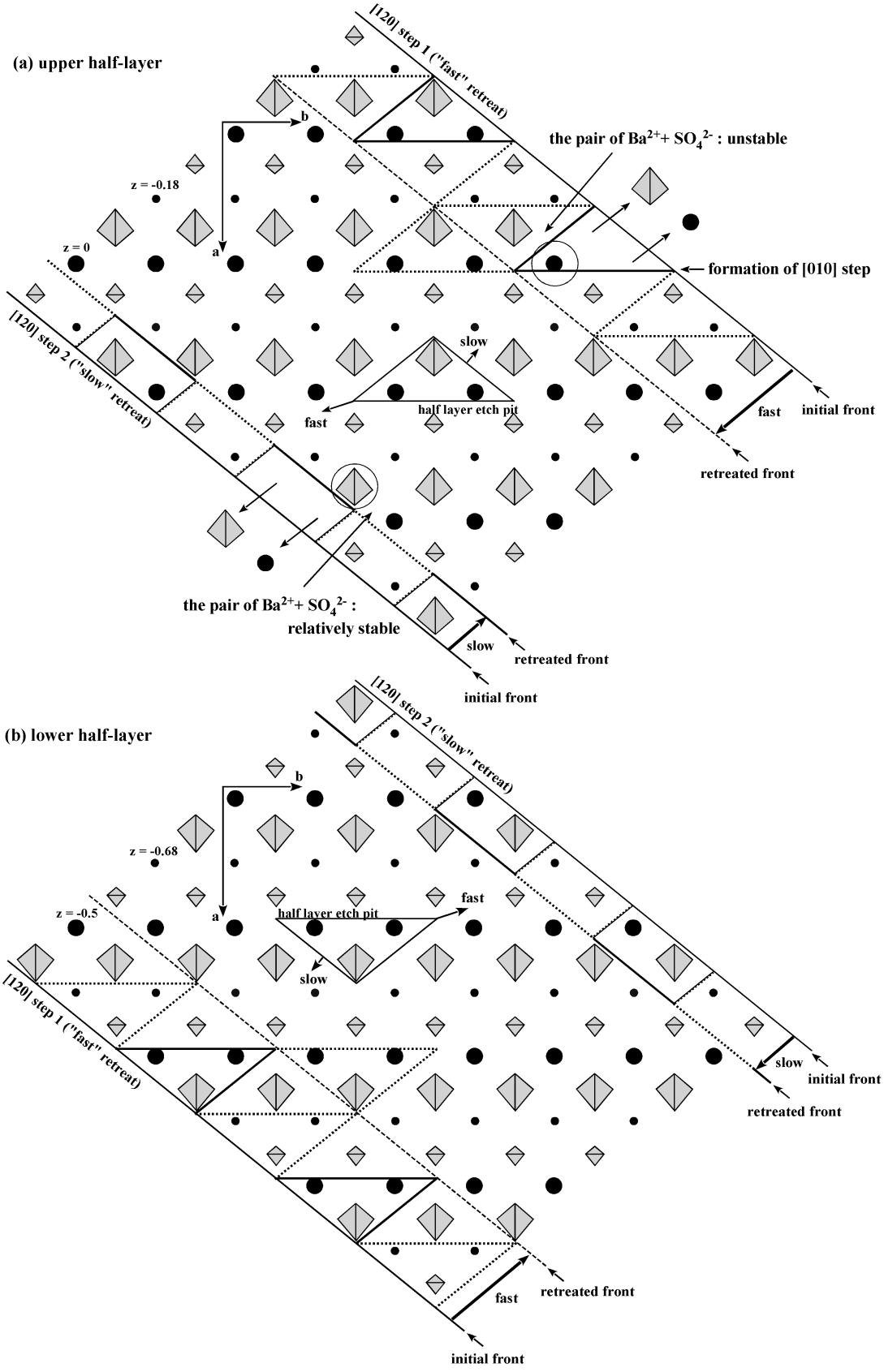
(a) upper half-layer
[120] step 1 ("fast" retreat)
b
a
z = -0.18
z = 0
the pair of Ba^{2+}+ SO_4^{2-} : unstable
formation of [010] step
[120] step 2 ("slow" retreat)
slow
fast
half layer etch pit
fast
initial front
retreated front
the pair of Ba^{2+}+ SO_4^{2-} :
relatively stable
slow
retreated front
initial front
(b) lower half-layer
[120] step 2 ("slow" retreat)
b
a
z = -0.68
z = -0.5
half layer etch pit
fast
slow
[120] step 1 ("fast" retreat)
slow
initial front
retreated front
fast
retreated front
initial front

Figure 6.

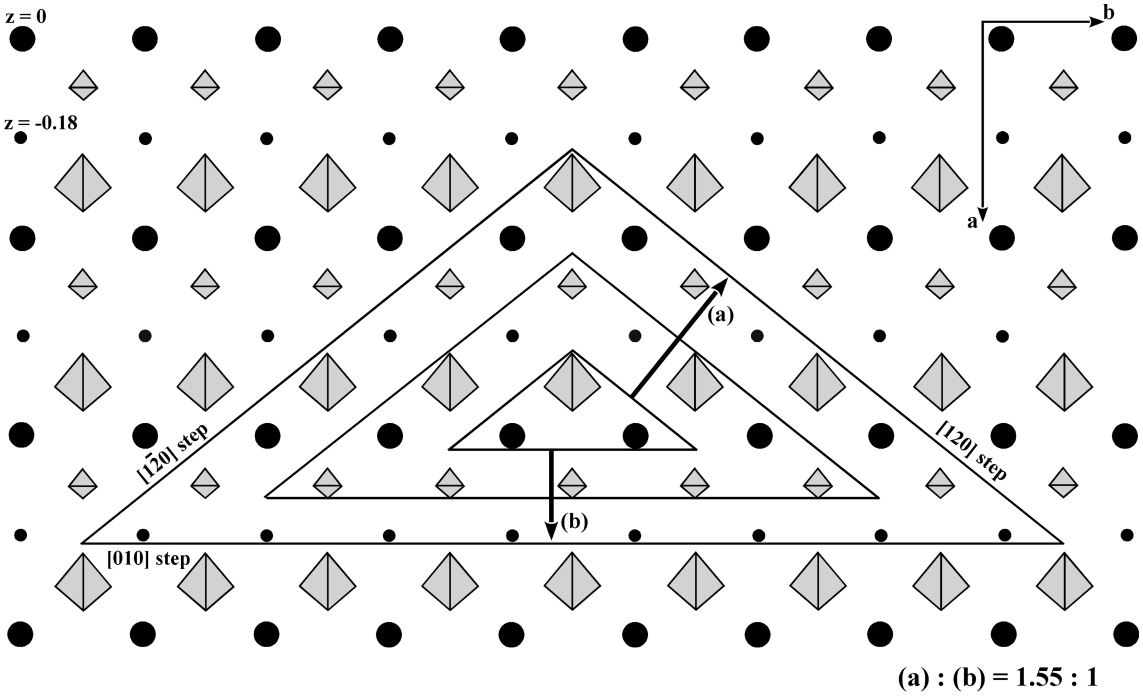

Figure 7.